Naphthalimide-based nonionic sulfonate photoacid generators: Structure-property relationship and sub-30nm resolution lithography

Changchang Zhuang,[†a] Jiao Chen,[†a] Tao Wang,[a] Jun Zhao,[b] Haoyuan Li,[a] Hanshen Xin*[a] and Jianhua Zhang*[a]

[a] School of Microelectronics, Shanghai Engineering Research Center for Integrated Circuits and Advanced Display Materials, Shanghai University, Shanghai, China

[b] Shanghai Synchrotron Radiation Facility, Shanghai Advanced Research Institute, Chinese Academy of Sciences, Shanghai, China

[†] Theses authors contributed equally

Corresponding Author(s): xinhanshen@shu.edu.cn; jhzhang@oa.shu.edu.cn

Contents

1. General information

4-Bromo-1,8-naphthalic Anhydride, 4-Methoxythiophenol, 4-tert-butylbenzenethiol, 4-Fluorothiophenol, tosyl chloride, and 4-(Trifluoromethyl) benzene-1-sulfonyl chloride were purchased form Titan Reagents. Dichloromethane (DCE), propylene glycol methyl ether acetate (PGMEA), tetrahydrofuran (THF), N, N-Dimethylformamide (DMF), potassium carbonate, hydroxylamine, triethylamine, acetonitrile, RB, and other organic solvents were obtained from Sinopharm Chemical Reagent Co., LTD., and no additional processing was done prior to use.

^{1}H NMR and ^{13}C NMR studies were performed on a JEOL JNM ECX 400 MHz spectrometer. Mass spectrometry (MS) measurements were recorded on a Thermo Fischer DART-MS spectrometer. Thermogravimetric analysis (TGA) measurements were conducted using a NETZSCH TG209F3 Tarsus Series instrument with a temperature range of 30 ℃ to 500 ℃ and a heating rate of 10 ℃/min in a nitrogen atmosphere. A NETZSCH DSC200F3 was used to perform differential scanning calorimetry (DSC) measurements spanning a temperature range from 30 ℃ to 260 ℃ with a heating rate of 10 ℃/min in a nitrogen environment at a heating rate of 10 ℃/min.

Spectral absorption measurements were carried out using a PerkinElmer 2D Detector Module UV spectrophotometer. Steady-state fluorescence spectra were collected using an Edinburgh FLS 1000 fluorescence spectrometer. The acid generation quantum yields were measured using a CME-SEB 500 mercury lamp apparatus under

irradiation at 254 nm. All PAG dissolved in acetonitrile were pre-gassed with N_2. The photic acid production process was monitored by PerkinElmer 2D Detector Module UV spectrophotometer. RB was used as a sensor for photoacid production and acid production in acetonitrile was assessed from a standard curve of RB, with the incident light intensity measured using a CME-FZ-A UV irradiometer.

The thickness of the films was measured using a J.A. Wollman Co. INC M-2000V ellipsometer or Filmetrics F50. 365 nm exposure experiments were carried out using a PLS-LED 100C tool (365 nm single wavelength). 254 nm exposure experiments were carried out using a CME-SEB 500 mercury lamp apparatus. A CABL-9500C system (voltage: 50 keV) was used for EBL. Optical images were captured using Keyence VK-X3000 white light interference laser microscope. A Regulus 8230 cold field emission scanning electron microscope (CFE-SEM) running at 0.5 keV acceleration voltage was used for examining the nanopatterns.

All calculations were carried out using the Gaussian 16 software (B.01).

2. General procedure for the synthesis of PAGs

2.1 Synthesis of 6-((4-methoxyphenyl)thio)-1,3-dioxo-1H-benzo[de]isoquinolin-2(3H)-yl 4-methylbenzenesulfonate (1a)

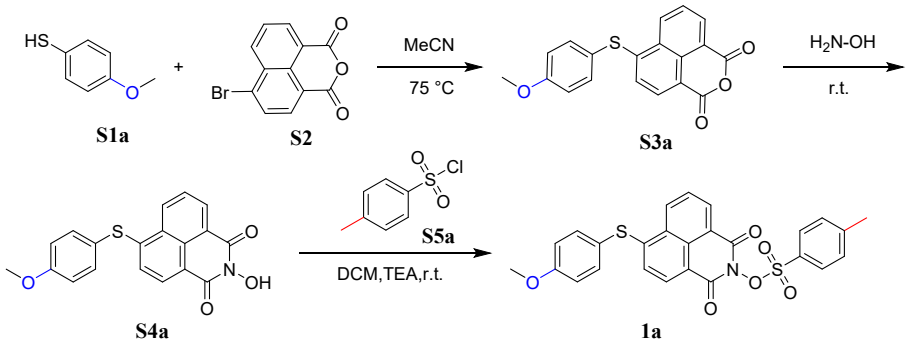

2.8 g (0.01 mol) of 4-bromo-1,8-naphthalic anhydride (S2) and 1.506 g (0.01 mol) of potassium carbonate were dissolved in 51 mL (0.97 mol) of acetonitrile, followed by the addition of 2.484 mL (0.02 mol) of p-methoxythiophenol (S1a). The mixture was reacted at 75 ℃ for 6 h to obtain intermediate S3a. Then add 1.67 mL (0.054 mol) of 50% hydroxylamine aqueous solution dropwise and react at room temperature for 2 h. Slowly pour the solution into water, add hydrochloric acid dropwise to pH=5, filter, and dry the obtained light yellow solid intermediate S4a at 70 ℃. Dissolve intermediate S4a in dichloromethane, add triethylamine, cool the mixture to 0 ℃, and add 0.457g (0.024mol) of p-toluenesulfonyl chloride (S5a) dropwise through a constant pressure dropping funnel. The reaction was stirred at room temperature overnight. The reaction mixture was quenched by addition of DI water. The aqueous layer was separated and extracted with ethyl acetate. The organic layers were combined, washed with brine, dried over $MgSO_4$, filtered and concentrated in vacuo. The crude product was purified by flash column chromatography rapidly to afford PAG 1a. Yield: 85.3%. ^{1}H NMR (400 MHz, Chloroform-d) δ 8.74-8.63 (m, 2H), 8.31 (d, J = 8.0 Hz, 1H), 8.03 (d, J = 8.1 Hz, 2H), 7.82 (t, J = 7.9 Hz, 1H), 7.54 (d, J = 8.7 Hz, 2H), 7.41 (d, J = 8.2 Hz, 2H), 7.11-6.96 (m, 3H), 3.90 (s, 3H), 2.49 (s, 3H). 13C NMR (101 MHz, Chloroform-d) δ 161.69, 160.11, 160.00, 150.06, 146.72, 133.02, 132.53, 132.24, 131.20, 130.16, 129.81, 129.03, 128.08, 127.21, 123.85, 123.05, 118.77, 116.31, 55.87, 22.25. HRMS (ESI): m/z calculated for $C_{26}H_{19}NO_6S_2$ $[M+H]^+$ 505.0654, found 505.5590.

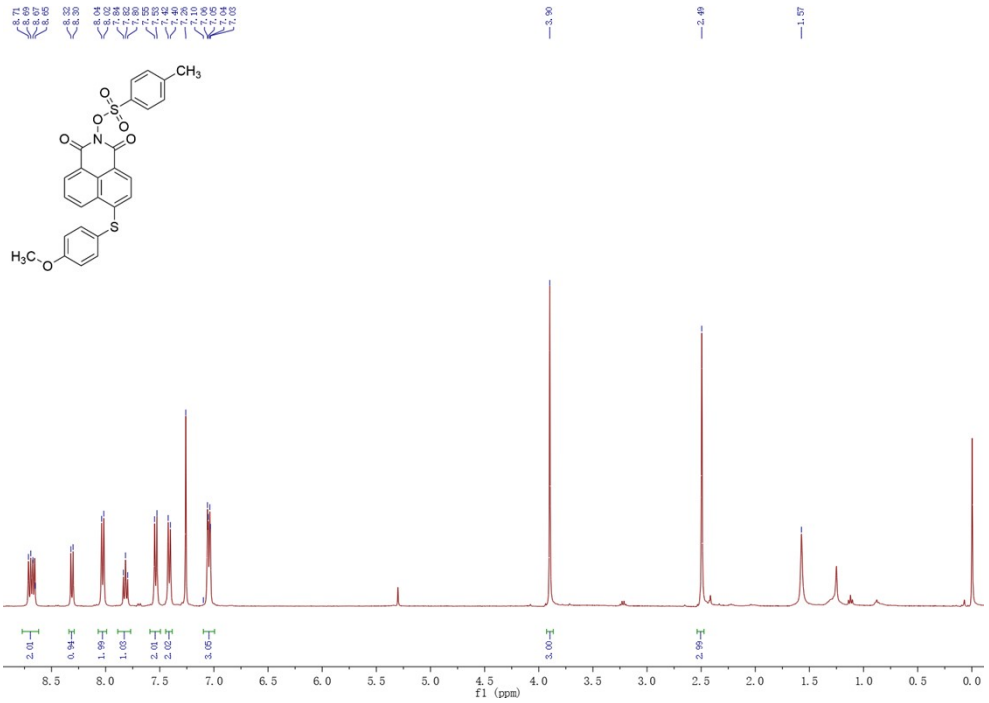

Fig. S1. ^{1}H NMR spectrum of PAG 1a in $CDCl_3$.

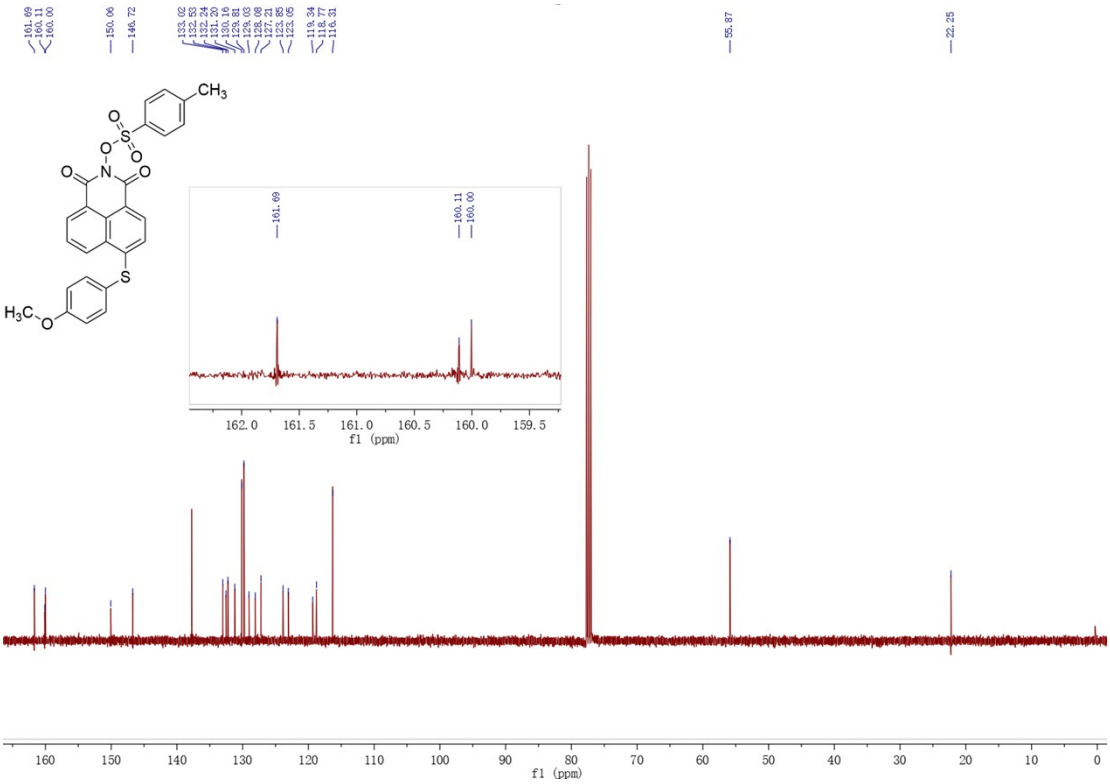

Fig. S2. ^{13}C NMR spectrum of PAG 1a in $CDCl_3$.

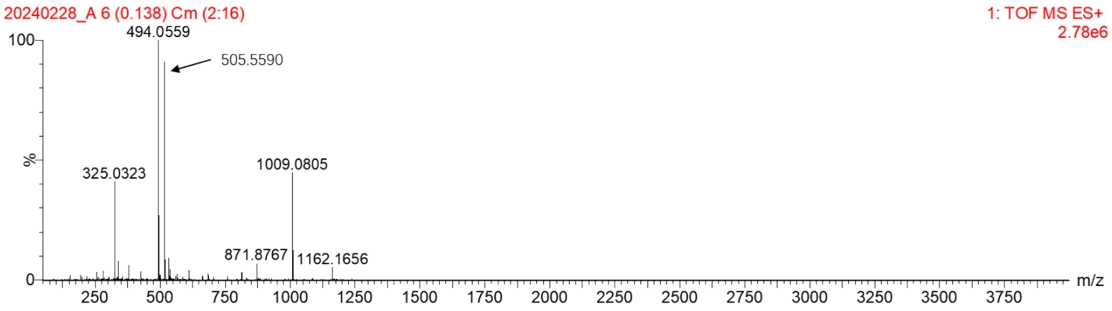

Fig. S3. HRMS spectrum of PAG 1a in $CDCl_3$.

2.2 Synthesis of 6-((4-(tert-butyl)phenyl)thio)-1,3-dioxo-1H-benzo[de]isoquinolin-2(3H)-yl 4-methylbenzenesulfonate (1b)

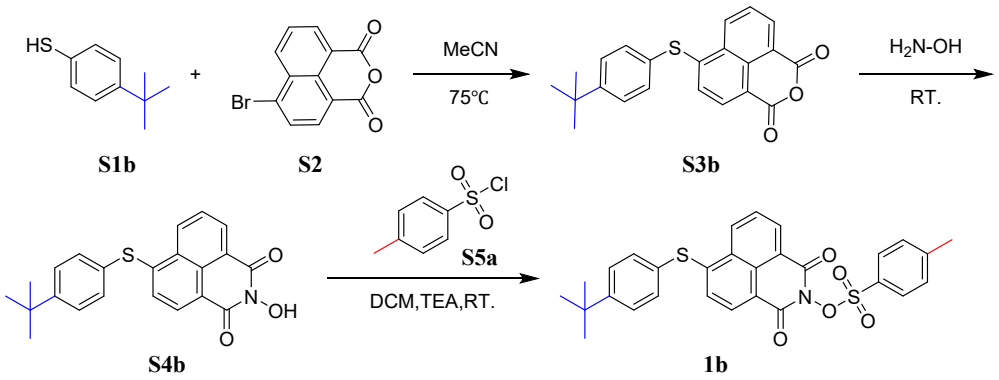

The synthesis method of PAG 1b is consistent with that of PAG 1a, in which p-methoxyphenylthiophenol (S1a) is replaced with p-tert butylphenylthiophenol (S1b). Yield: 83.6%. ^{1}H NMR (400 MHz, Chloroform-d) δ 8.73 (d, J = 8.5 Hz, 1H), 8.66 (d, J = 7.3 Hz, 1H), 8.34 (d, *J* = 8.0 Hz, 1H), 8.03 (d, *J* = 8.4 Hz, 2H), 7.81 (t, *J* = 7.9 Hz, 1H), 7.52 (s, 4H), 7.41 (d, *J* = 8.0 Hz, 2H), 7.17 (d, *J* = 8.0 Hz, 3H), 2.49 (s, 3H), 1.38 (s, 9H). ^{13}C NMR (101 MHz, Chloroform-d) δ 160.10, 159.98, 148.97, 146.73, 135.24, 133.04, 132.52, 132.25, 131.44, 130.16, 129.82, 129.42, 128.14, 127.75, 127.30, 126.12, 124.89, 123.07, 119.13, 35.27, 31.56, 22.25. HRMS (ESI): m/z calculated for $C_{29}H_{25}NO_5S_2$ $[M+H]^+$ 532.1247, found 532.1257.

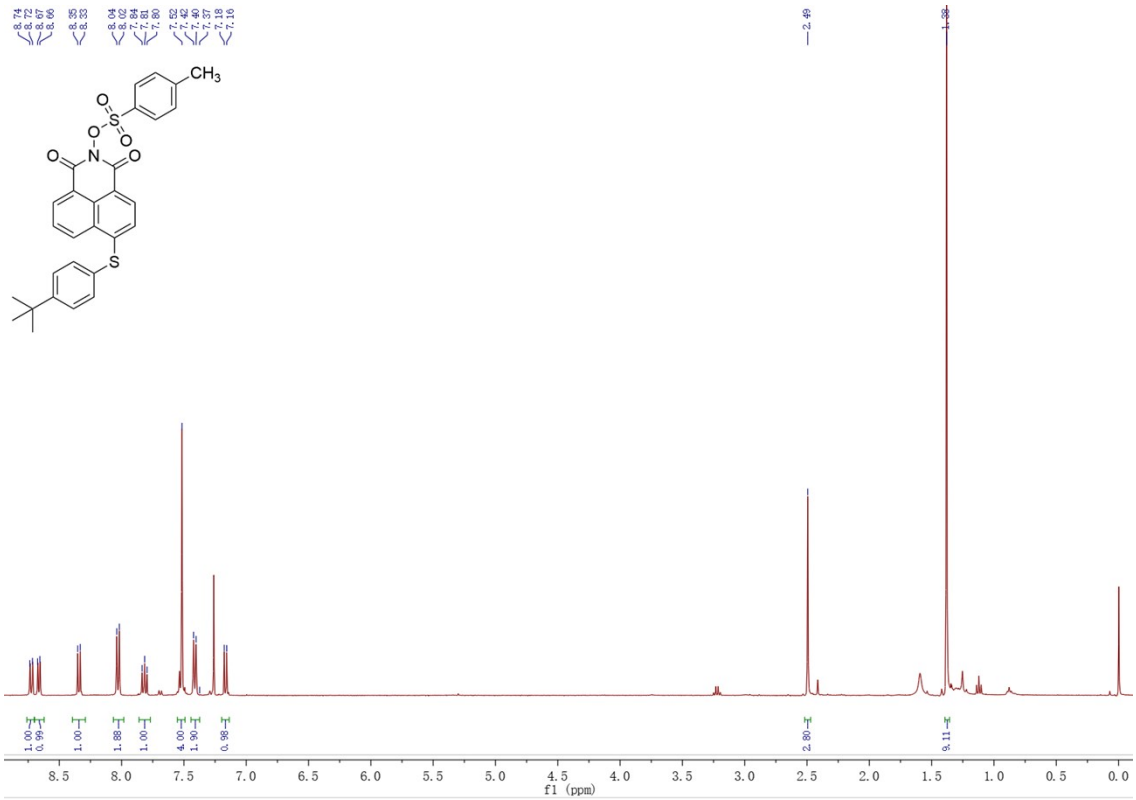

Fig. S4. ^{1}H NMR spectrum of PAG 1b in $CDCl_3$.

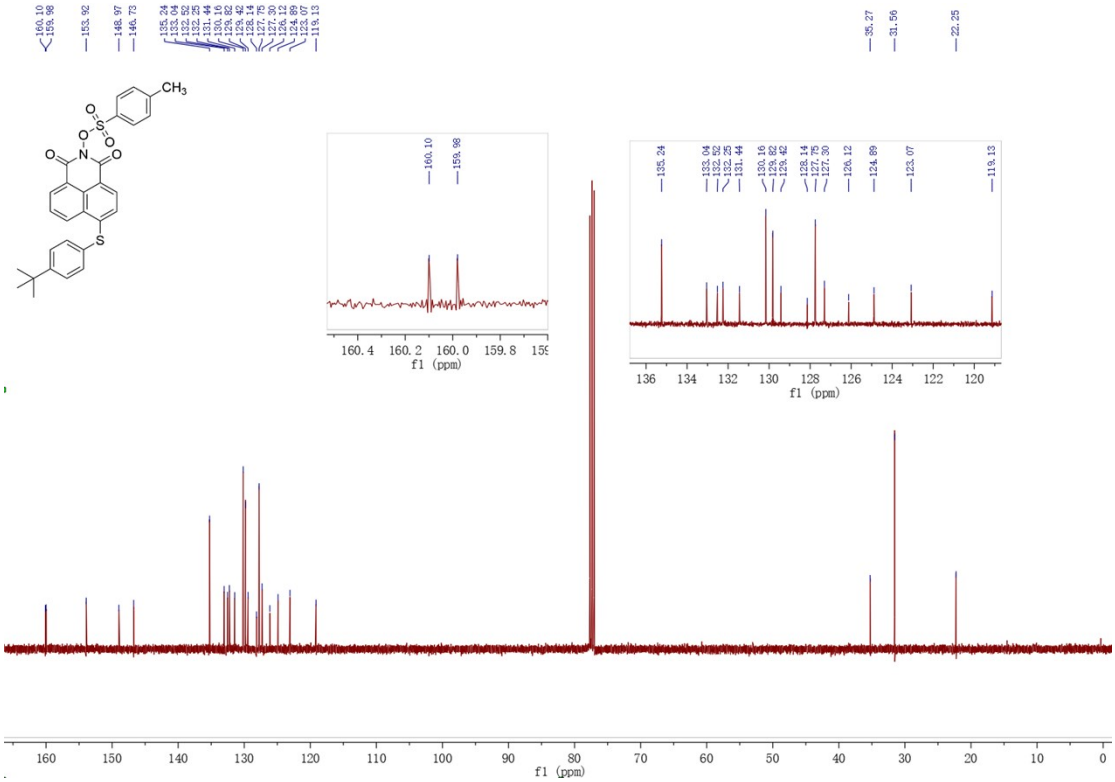

Fig. S5. ^{13} C NMR spectrum of PAG 1b in $CDCl_3$.

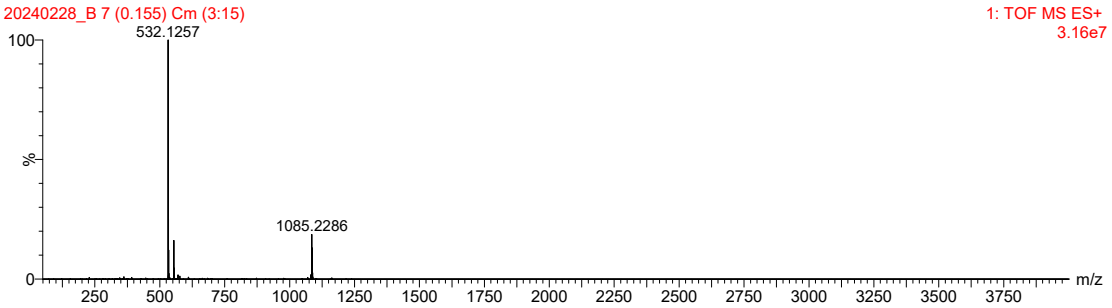

Fig. S6. HRMS spectrum of PAG 1b in $CDCl_3$.

2.3 Synthesis of 6-((4-fluorophenyl)thio)-1,3-dioxo-1H-benzo[de]isoquinolin-2(3H)-yl 4-methylbenzenesulfonate (1c)

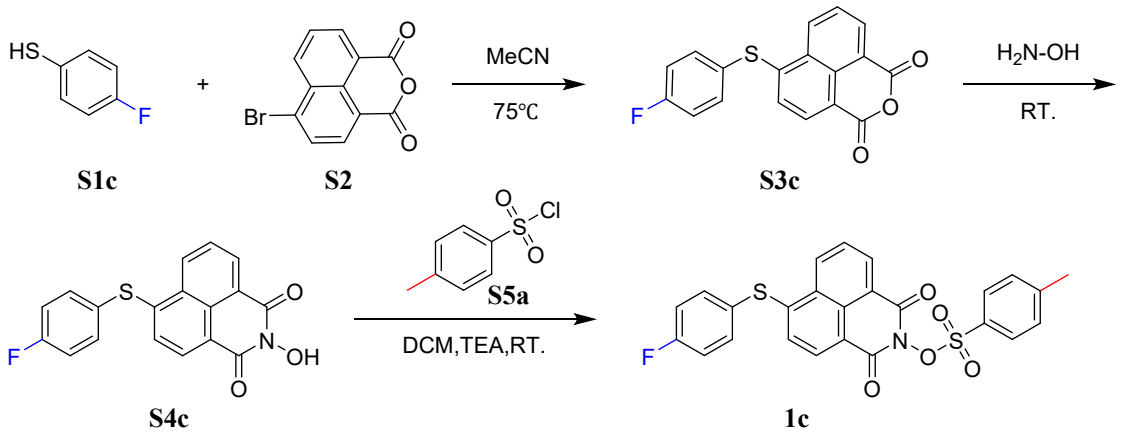

The synthesis method of PAG 1c is consistent with that of PAG 1a, in which p-methoxyphenylthiophenol (S1a) is replaced with p-fluorophenylthiophenol (S1c). Yield: 84.5%. ^{1}H NMR (400 MHz, Chloroform-*d*)) δ 8.69 (t, *J* = 8.3 Hz, 2H), 8.35 (d, *J* = 8.0 Hz, 1H), 8.03 (d, *J* = 8.0 Hz, 2H), 7.83 (t, *J* = 7.9 Hz, 1H), 7.58 (dd, *J* = 8.3, 5.1 Hz, 2H), 7.42 (d, *J* = 8.0 Hz, 2H), 7.21 (t, *J* = 8.3 Hz, 3H), 7.13 (d, *J* = 8.0 Hz, 1H), 2.50 (s, 3H). ^{19}F NMR (376 MHz, Chloroform-*d*) δ -109.60 (m). ^{13}C NMR (101 MHz, Chloroform-*d*) δ165.24, 162.73, 160.29, 148.52, 146.44, 137.62, 137.54, 133.81, 132.89, 132.78, 131.4 (d, *J* = 88 Hz), 131.16, 129.82, 129.46, 127.32, 127.14, 124.61, 124.29, 119.26 (d, *J* = 12 Hz), 117.87, 117.65, 115.34, 21.88. HRMS (ESI): m/z calculated for $C_{25}H_{16}FNO_5S_2$ $[M+H]^+$ 494.0527, found 494.0559.

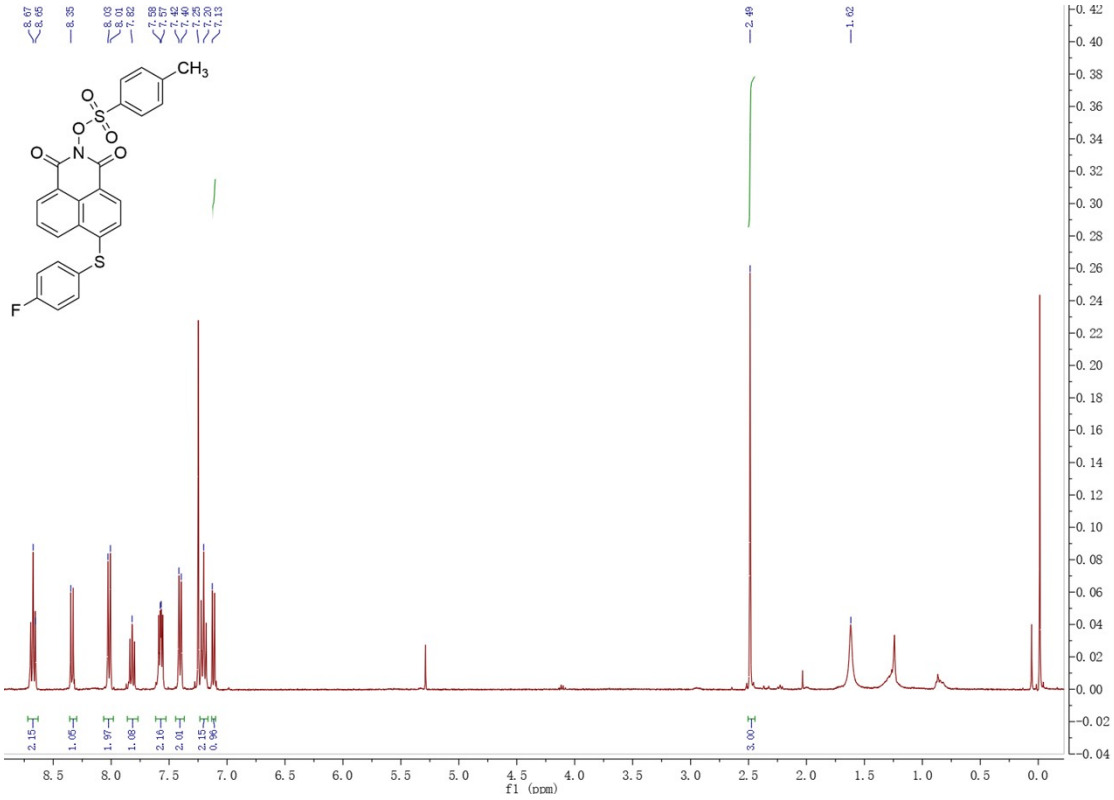

Fig. S7. ^{1}H NMR spectrum of PAG 1c in $CDCl_3$.

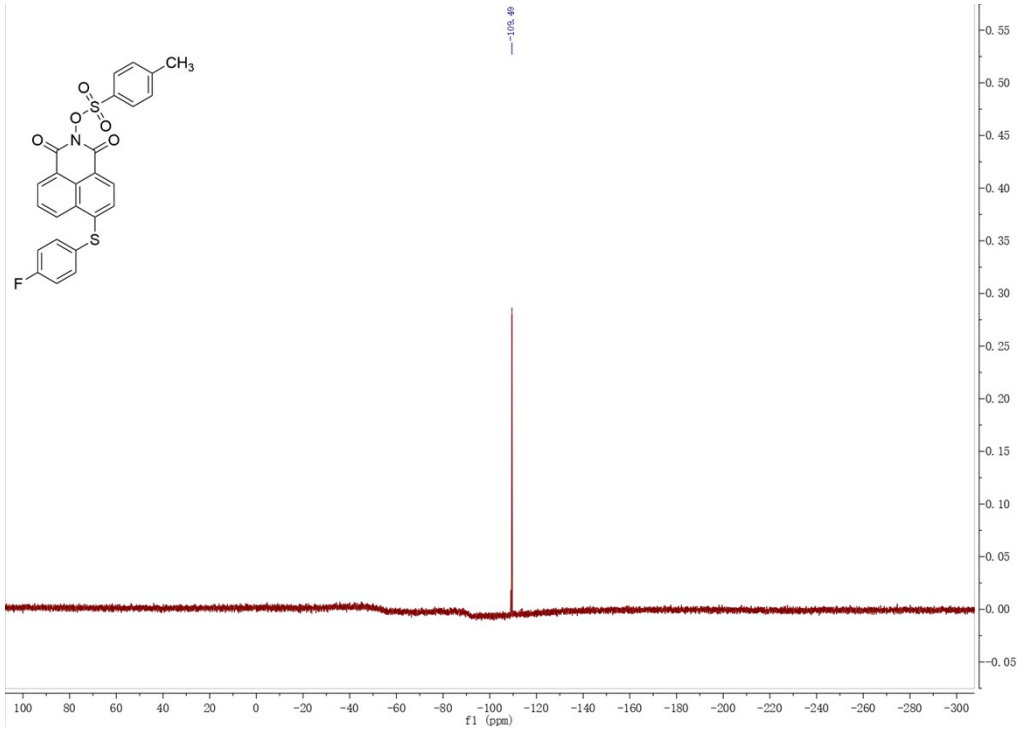

Fig. S8. ^{19}F NMR spectrum of PAG 1c in $CDCl_3$.

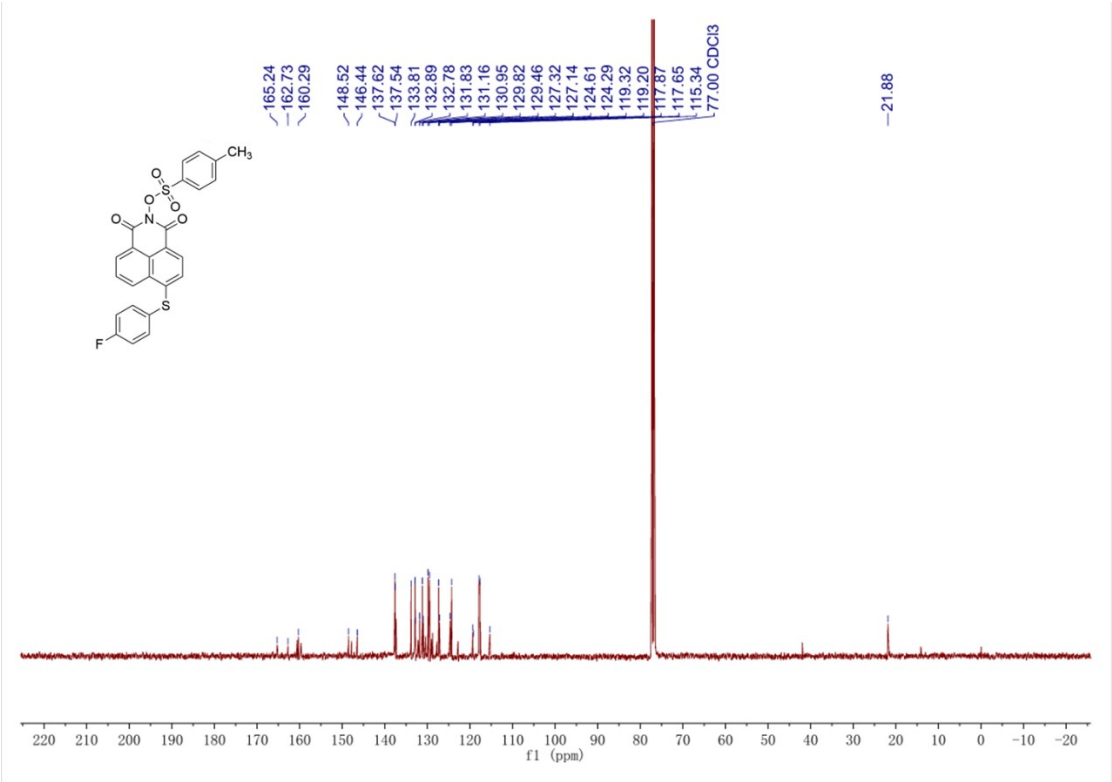

Fig. S9. ^{13}C NMR spectrum of PAG 1c in $CDCl_3$

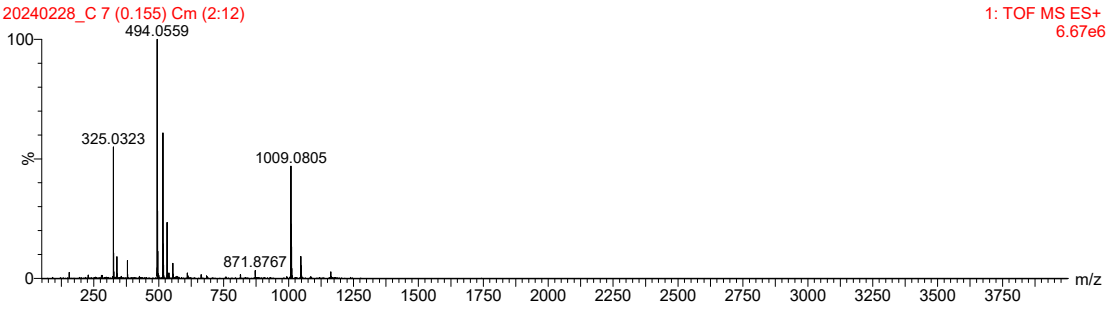

Fig. S10. HRMS spectrum of PAG 1c in $CDCl_3$.

2.4 Synthesis of 6-((4-methoxyphenyl)thio)-1,3-dioxo-1H-benzo[de]isoquinolin-2(3H)-yl 4-(trifluoromethyl)benzenesulfonate (1d)

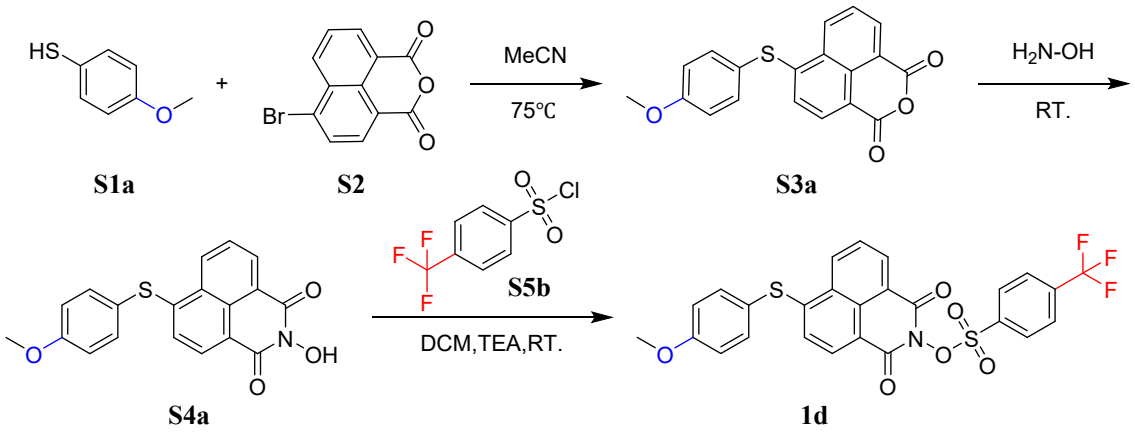

The synthesis method of PAG 1d is consistent with that of PAG 1a, in which p-toluenesulfonyl chloride (S5a) is replaced with trifluorobenzenesulfonyl chloride (S5b). Yield: 91.2%. ^{1}H NMR (400 MHz, Chloroform-*d*) δ 8.72 (d, *J* = 9.6 Hz, 1H), 8.67 (d, *J* = 8.5 Hz, 1H), 8.32-8.27 (m, 3H), 7.89 (d, *J* = 8.5 Hz, 2H), 7. 83 ((t, *J* = 7.9 Hz, 1H), 7.54 (d, *J* = 8.8 Hz, 3H), 7.11-7.01 (m, 3H), 3.90 (s, 3H). ^{19}F NMR (376 MHz, Chloroform-*d*) δ -63.19. ^{13}C NMR (101 MHz, Chloroform-*d*) δ 161.52, 159.75, 159.63, 150.36, 139.06, 137.54, 136.46 (q, *J* = 33.3 Hz), 132.93, 132.13, 131.17, 130.07, 128.76, 127.80, 127.02, 126.37 (q, *J* = 3.7 Hz), 123.51 (q, *J* = 274.7 Hz), 123.56, 122.53, 118.87, 118.16, 116.11, 55.62. HRMS (ESI): m/z calculated for $C_{26}H_{16}F_3NO_6S_2$ $[M+H]^+$ 560.0444, found 560.0466.

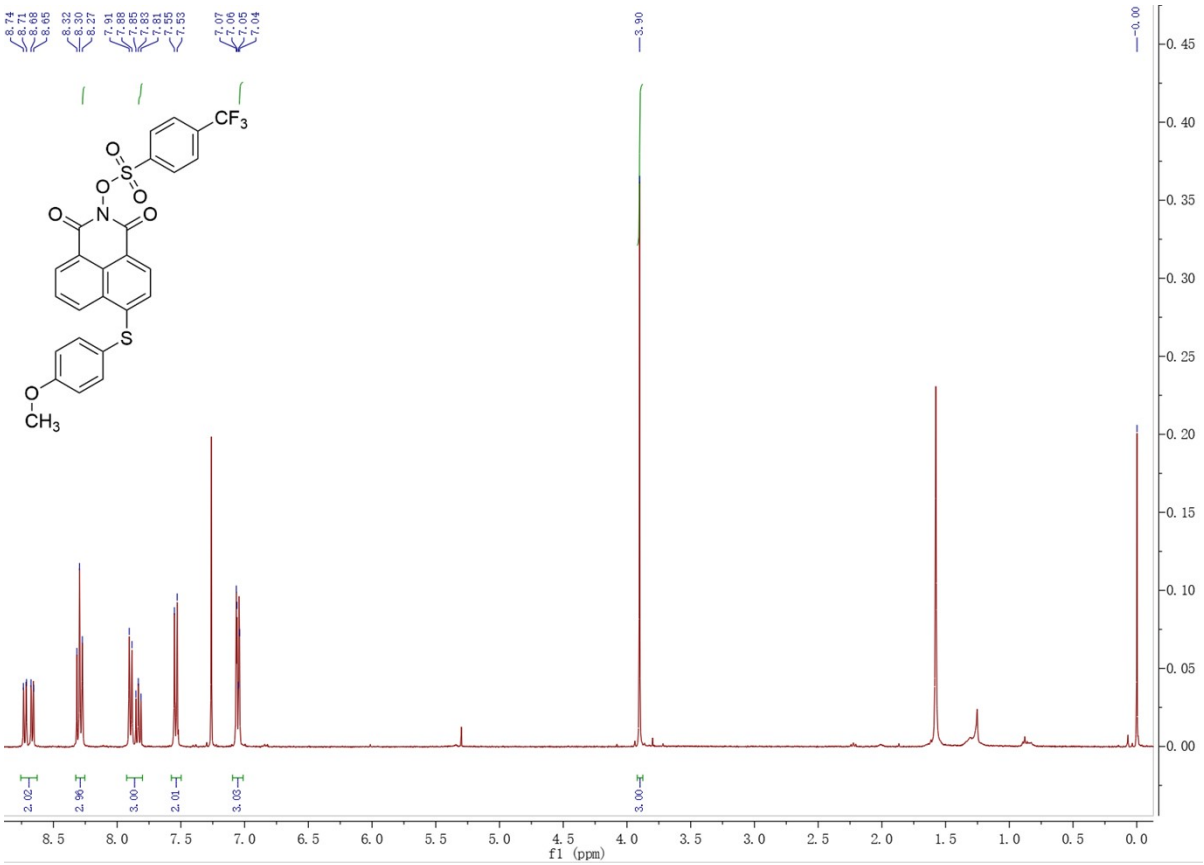

Fig. S11. ^{1}H NMR spectrum of PAG 1d in $CDCl_3$.

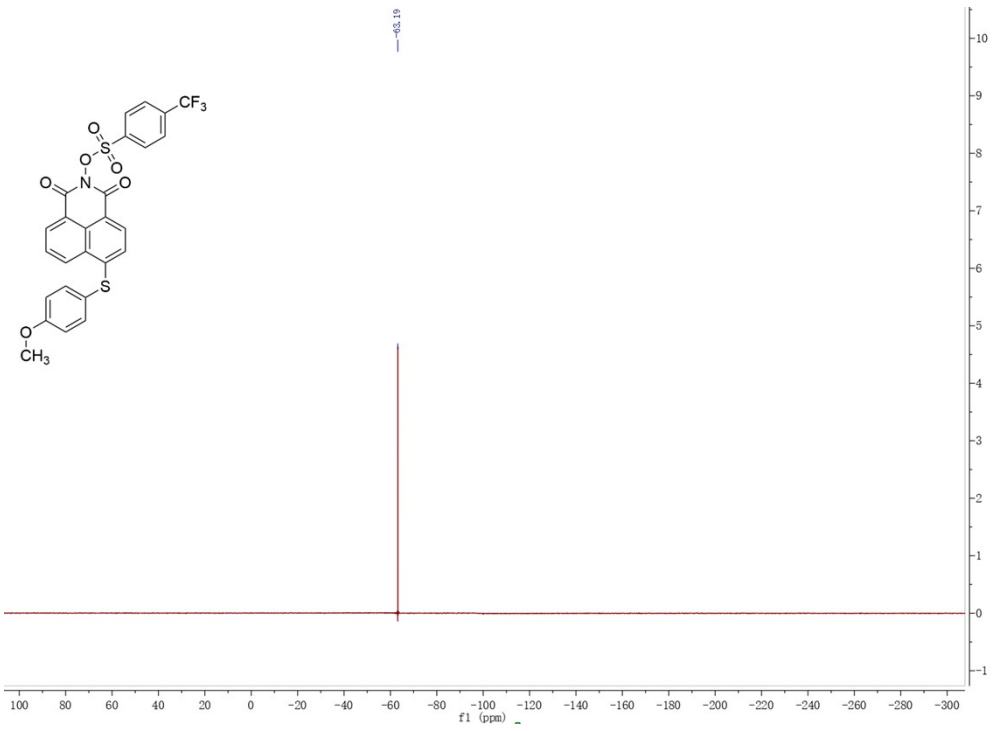

Fig. S12. ^{19}F NMR spectrum of PAG 1d in $CDCl_3$.

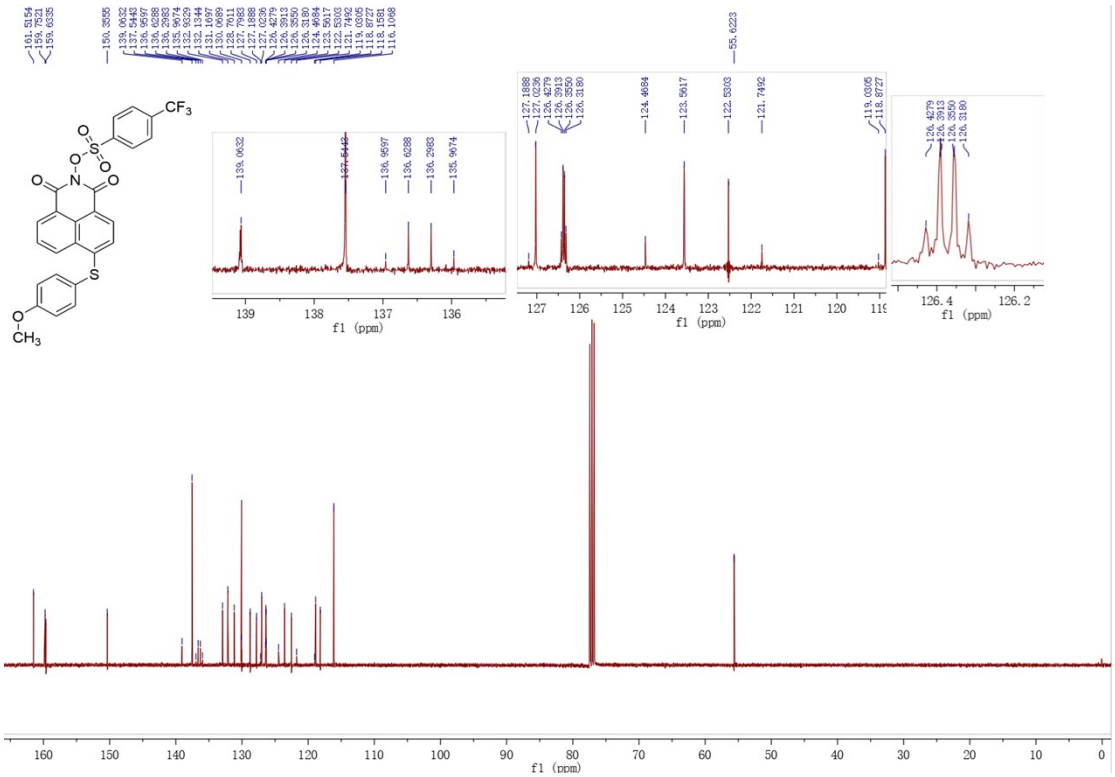

Fig. S13. ^{13}C NMR spectrum of PAG 1d in $CDCl_3$.

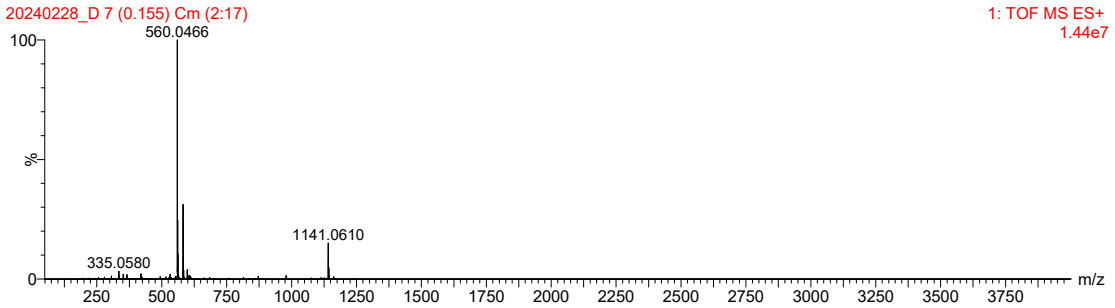

Fig. S14. HRMS spectrum of PAG 1d in $CDCl_3$.

2.5 Synthesis of 6-((4-methoxyphenyl)thio)-1,3-dioxo-1H-benzo[de]isoquinolin-2(3H)-yl 4-methoxybenzenesulfonate (1e)

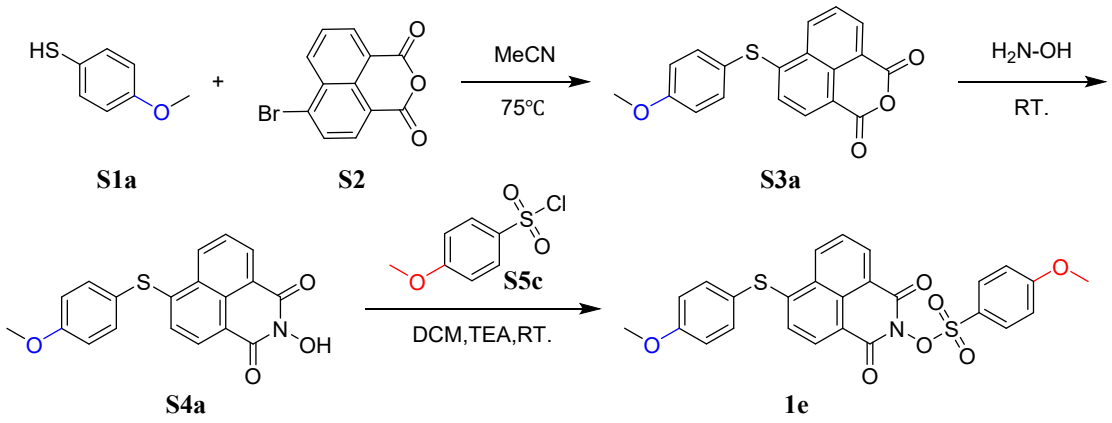

The synthesis method of PAG 1e is consistent with that of PAG 1a, in which p-toluenesulfonyl chloride (S5a) is replaced with 4-methoxybenzenesulfonyl chloride (S5c). Yield: 87.4%. ^{1}H NMR (400 MHz, Chloroform-*d*) δ 8.69 (dd, *J* = 8.5, 1.1 Hz, 1H), 8.65 (dd, *J* = 8.6, 1.1 Hz, 1H), 8.30 (d, *J* = 8.0 Hz, 1H), 8.08 (d, *J* = 9.2 Hz, 2H), 7.80 (dd, *J* = 8.5, 7.3 Hz, 1H), 7.52 (d, *J* = 8.9 Hz, 2H), 7.08-6.95 (m, 5H), 3.91 (s, 3H), 3.89 (s, 4H). ^{13}C NMR (101 MHz, Chloroform-*d*) δ 165.20, 161.68, 160.14, 160.03, 150.01, 137.74, 132.98, 132.25, 132.20, 131.15, 128.99, 128.05, 127.20, 126.47, 123.83, 123.05, 119.33, 118.78, 116.30, 114.74, 56.13, 55.86. HRMS (ESI): m/z calculated for $C_{26}H_{19}NO_7S_2$ $[M+H]^+$ 522.0676, found 522.0656.

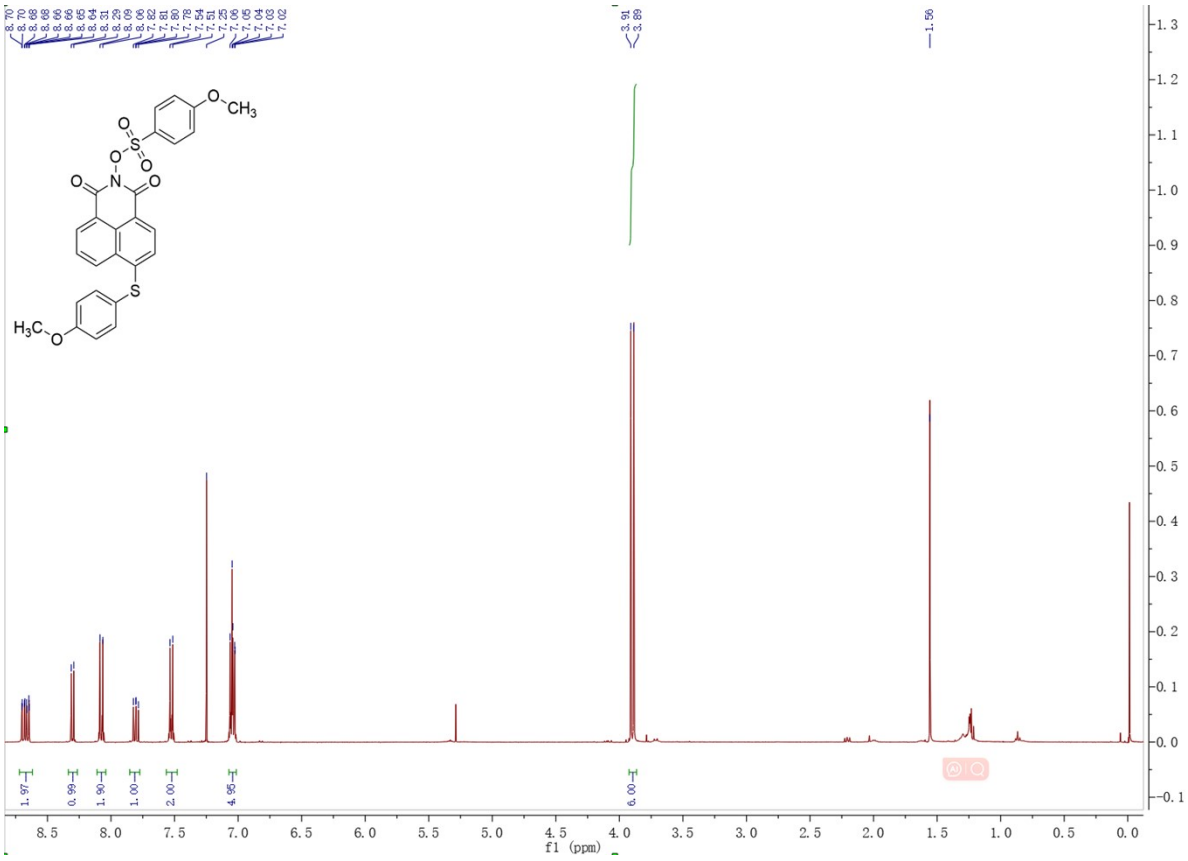

Fig. S15. ^{1}H NMR spectrum of PAG 1e in $CDCl_3$.

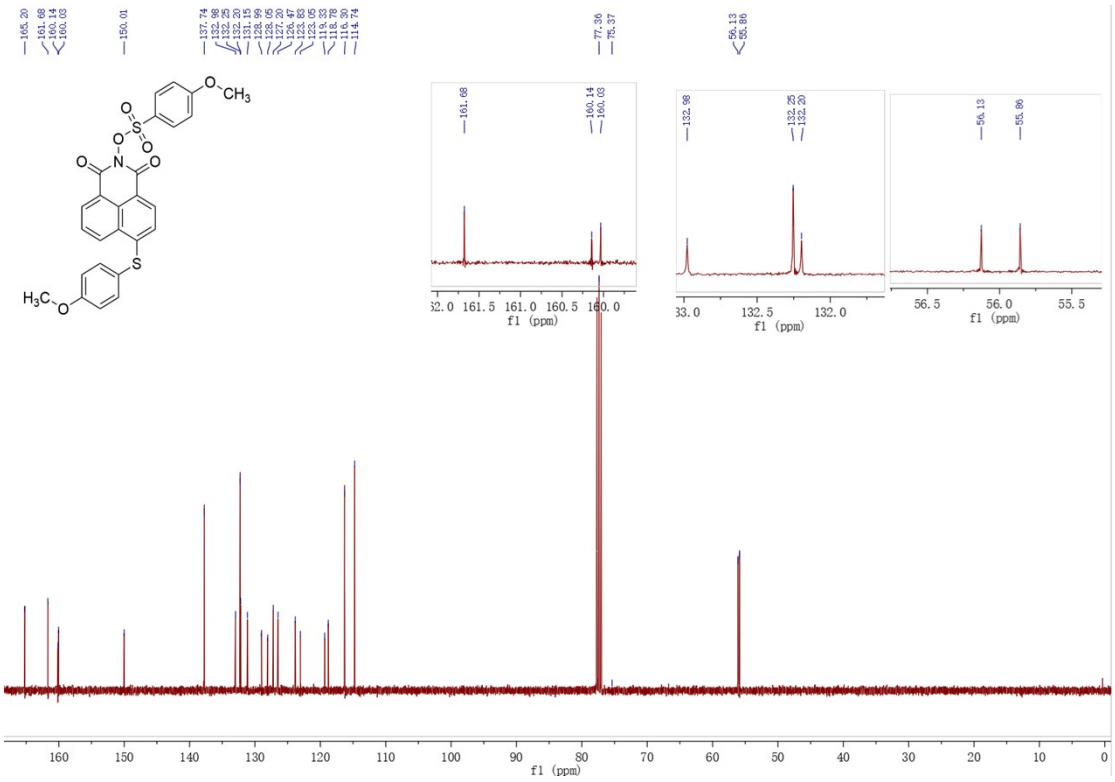

Fig. S16. ^{13}C NMR spectrum of PAG 1e in $CDCl_3$.

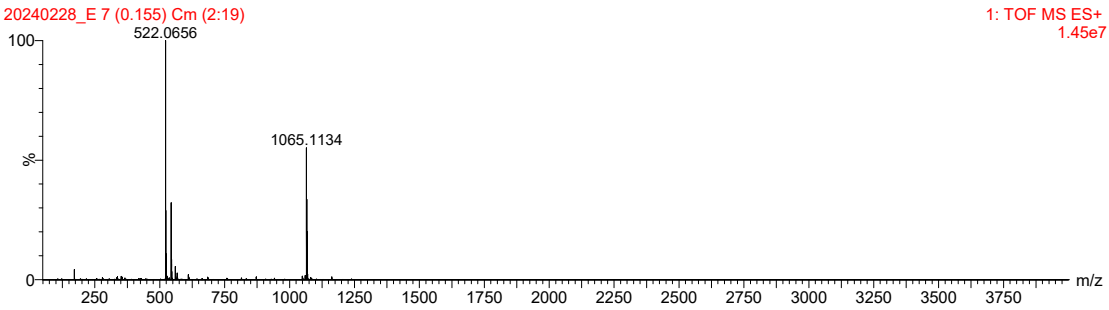

Fig. S17. HRMS spectrum of PAG 1e in $CDCl_3$.

3. Solubility test

Table S1. Solubility of PAGs 1a-1e

PAG	Methanol	acetone	Ethyl lactate	THF	ACN	1,4-dioxane	PGMEA	DMF	DCE
1a	--	-	+	++	-	+	-	++	++
1b	--	++	-	++	-	++	+	++	++
1c	--	+	+	++	-	++	+	++	++
1d	--	-	-	++	-	+	-	++	++
1e	--	-	-	+	-	+	-	++	++

Note：++ indicate above 30 mg/mL, + indicate 20-30 mg/mL, - indicate less than 10 mg/mL, -- indicate insoluble.

4. Thermal stability data of PAGs 1a-1e

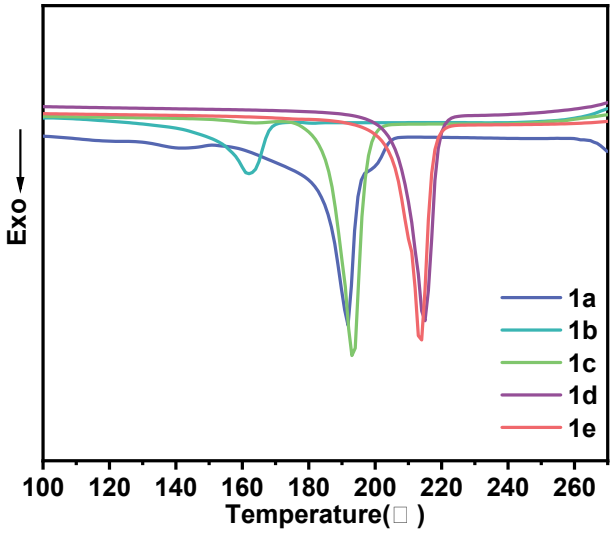

Fig. S18. DSC curves of PAGs 1a-e.

Table S2. Thermal stability data of PAGs 1a-1e

PAG	$T_{2wt\%}$/°C	$T_{5wt\%}$/°C	$T_{10wt\%}$/°C	Residual rate/wt% (600°C)	T_m/°C
1a	275.8	295.6	304.0	43.1	191.3
1b	268.2	296.6	307.2	23.7	161.8
1c	277.4	302.7	313.1	29.3	193.1
1d	266.8	282.6	292.9	40.9	215.2
1e	295.1	302.0	307.9	42.9	213.7

5. UV absorption data of PAGs 1a-1e

Table S3. UV absorption data of PAGs 1a-1e

PAG	λ_{max} (nm)	$Log\varepsilon_{max}$ [a]	$Log\varepsilon_{248}$ [a]	$Log\varepsilon_{254}$ [a]	$Log\varepsilon_{365}$ [a]
1a	232	4.929	4.514	4.453	4.173
1b	227	4.965	4.658	4.552	4.085
1c	220	4.925	4.605	4.587	4.445
1d	222	4.932	4.586	4.539	4.246
1e	235	4.983	4.875	4.812	4.301

[a]$Log\varepsilon_{max}$, $Log\varepsilon_{248}$, $Log\varepsilon_{254}$ and $Log\varepsilon_{365}$ represent the logarithm of the molar extinction coefficients at the wavelengths corresponding to the maximum absorption peak, 248 nm, 254 nm, and 365 nm, respectively.

6. Fluorescence spectrum of PAGs 1a-1e

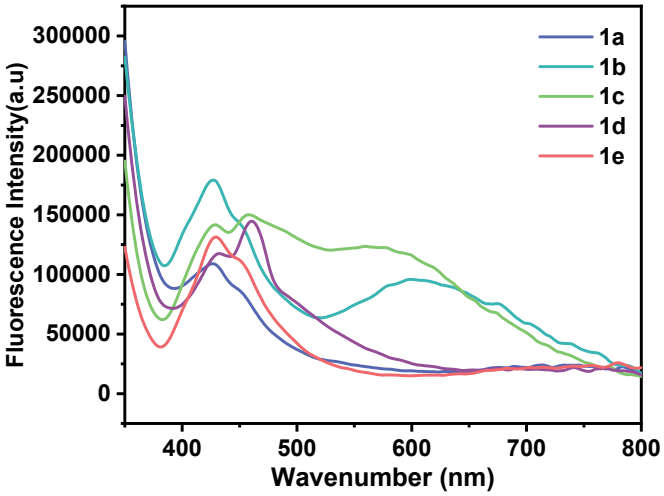

Fig. S19. Fluorescence spectrum of PAGs 1a-e.

7. Method for determining the acid production quantum yield of PAGs

7.1 Calibration of standard curves

Fig. S20 shows the curve of UV absorption of RB as a function of acid concentration. Using RB as an acid-sensitive indicator, it is dissolved in ultra-dry acetonitrile, and a series of target acids with gradually changing concentrations corresponding to PAG are added for reaction, resulting in an RB solution concentration of 2.0×10^{-5} M. The acid concentration increases from 0.5×10^{-5} to 3×10^{-5} M. By mixing a series of acids with different concentrations with a certain concentration of RB solution, it can be observed that as the acid concentration gradually increases, the color of the mixed solution deepens.

To quantitatively analyze this change process, the absorbance changes (ΔAbs) of RB under different concentration conditions were monitored using a UV-Vis spectrophotometer. Within a specific concentration range, the absorbance at 555 nm was plotted as the vertical axis and the concentration of the acid as the horizontal axis. This curve clearly shows that the characteristic absorption peak of RB (555 nm) exhibits a good linear relationship with the acid concentration, thus obtaining the so-called standard working curve. The slopes (K) of the three sulfonic acid standard curves corresponding to all PAGs are summarized in Table S4.

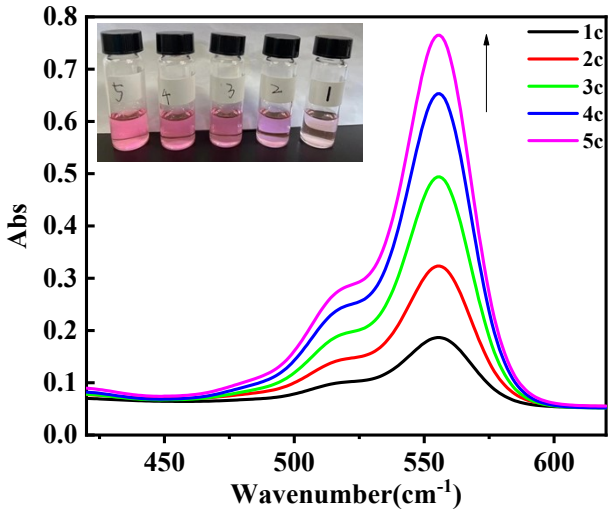

Fig. S20. Curve of UV absorption of RB with acid concentration

Table S4. Summary of standard working curve data for different sulfonic acid

Acid	Linear concentration range of acid	Linear range of absorbance	K	R^2
p-toluene sulfonic acid	0-0.02 mM	0-0.76	52.3	0.9996
Trifluoromethylbenzenesulfonic acid	0-0.02 mM	0-0.92	64.6	0.9991
p-methoxybenzenesulfonic acid	0-0.02 mM	0-0.68	45.8	0.9993

7.2 Detection of PAG acid production quantum yield

Dissolve PAG in ACN to prepare a solution with a concentration of 2.0×10^{-5} M, and expose it to a 254 nm mercury lamp light source. Collect exposed samples at different exposure time intervals (2 min, 4 min, 6 min, 8 min, 10 min, and 12 min), and thoroughly mix the exposed samples with RB acetonitrile solution with a concentration of 5.0×10^{-5} M Mix and measure the absorbance of the mixed solution at 555 nm, and record the change in light source exposure intensity (I). Use the unit exposure time as the horizontal axis and the corresponding absorbance change (ΔAbs) as the vertical axis for plotting. Draw the acid production kinetics curve of the photo induced acid generator and further calculate the slope (Ka) of the curve. Based on this slope, we accurately calculated the Φ_a of PAGs using formula (1).

$$\Phi_a = \left(\frac{3.98}{\lambda}\right)\frac{K_a}{\left[IK\left(1-10^{-A_\lambda}\right)\right]} \quad (1)$$

where K_a is the maximum slope of the acid production kinetic curve for exposure in PAGs solution, units: min^{-1}; λ is the exposure wavelength, units: nm; I is the exposure light intensity at a given wavelength λ, units: W/cm^2; A_λ is the absorbance of the solution at a given wavelength λ; and K is the slope of the standard operating curve for a given RB in a solvent and strong acid system.

This test was conducted three independent repeated experiments, and the final reported data in the article is the average of the three experiments.

8. Calculation from EBL Contrast Curves

Different numbers of 50 μm × 50 μm exposure patterns with different exposure doses were obtained by electron beam exposure and then developed by 2.38 % TMAH. The preserved film thickness of the square areas were measured by step profiler. Plot the contrast curve of the photoresist using exposure dose as the x-axis and normalized film thickness as the y-axis and perform logical function fitting. The normalized remaining thickness (NRT) scatter plots were fitted by logistic function as $y = \frac{A_1 - A_2}{1 + \left(\frac{x}{x_0}\right)^p} + A_2$ (a common S-shaped curve). The equation of the tangent at 0.5 (NRT=0.5) of the fitted line is calculated and E_0 was the calculated dose with NRT=0 while E_{100} was the calculated dose with NRT=1 by tangent equation. The definition of E_{100} was the higher dose required to totally retain the resist. E_0 was defined as the lower dose required to totally remove. The contrast value (γ) was derived from the following formula:

$$\gamma = \frac{1}{log\left(\frac{E_0}{E_{100}}\right)}$$

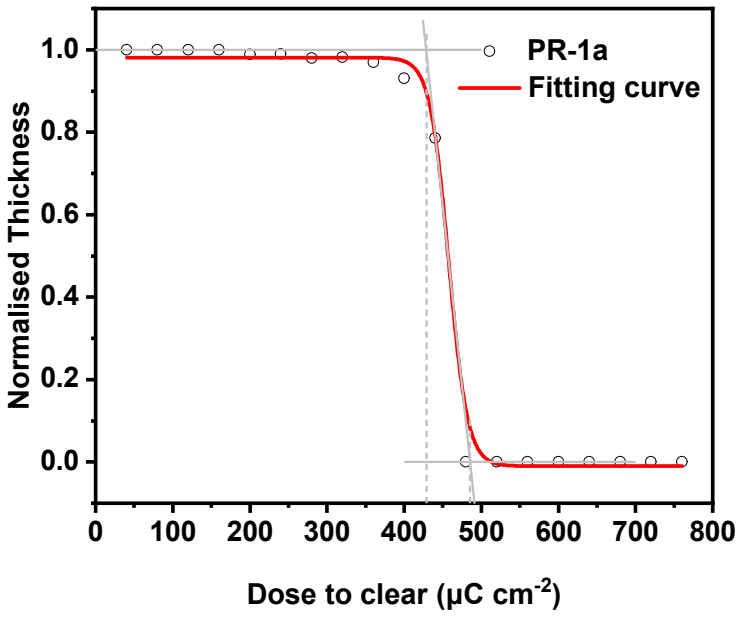

Fig. S21. The contrast curve of the PR-1a after exposed to the electron beam with different doses (40-760 μC cm^{-2}).

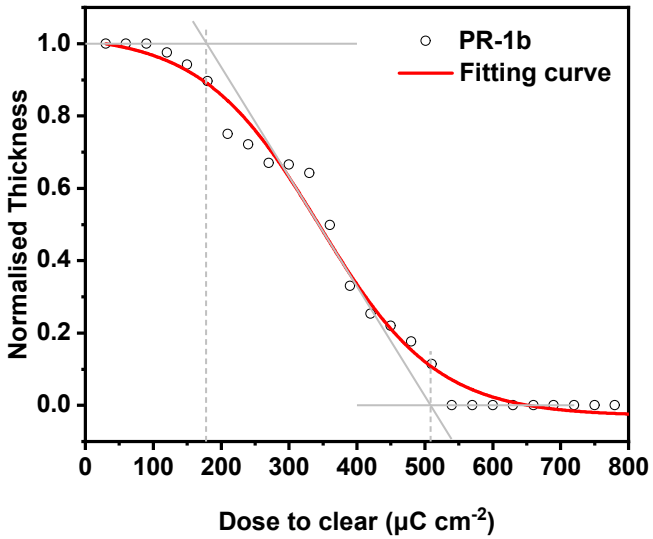

Fig. S22. The contrast curve of the PR-1b after exposed to the electron beam with different doses (30-810 μC cm^{-2}).

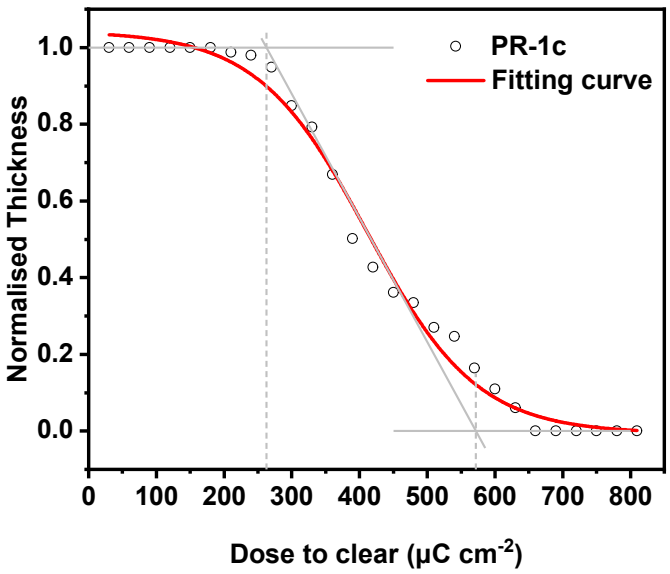

Fig. S23. The contrast curve of the PR-1c after exposed to the electron beam with different doses (30-810 μC cm^{-2}).

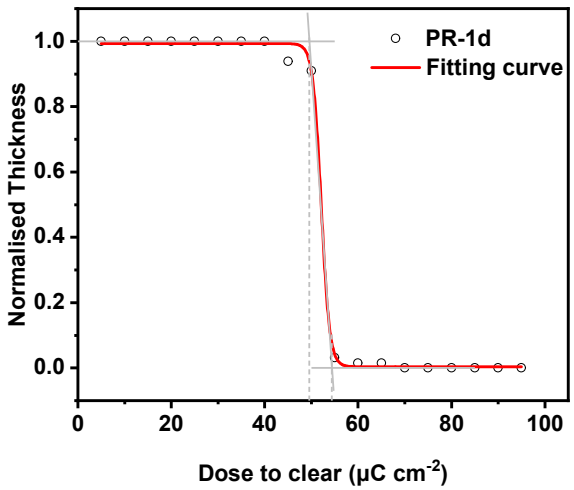

Fig. S24. The contrast curve of the PR-1d after exposed to the electron beam with different doses (5-95 μC cm^{-2}).

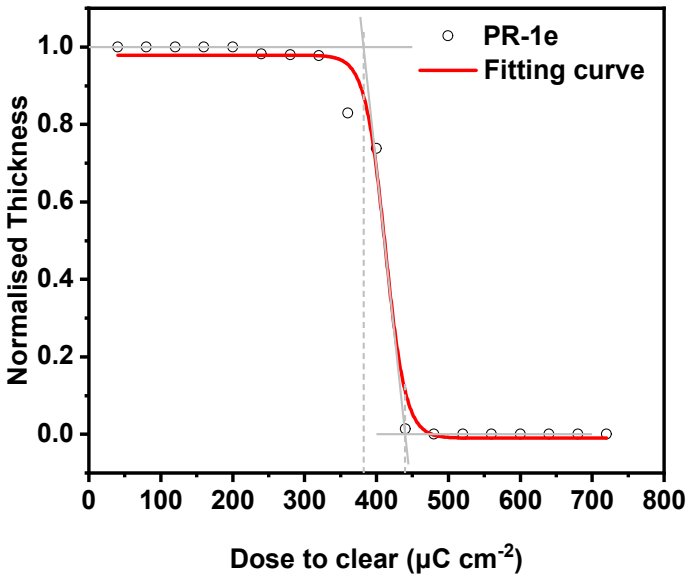

Fig. S25. The contrast curve of the PR-1e after exposed to the electron beam with different doses (40-760 μC cm^{-2}).

9. Exposure imaging

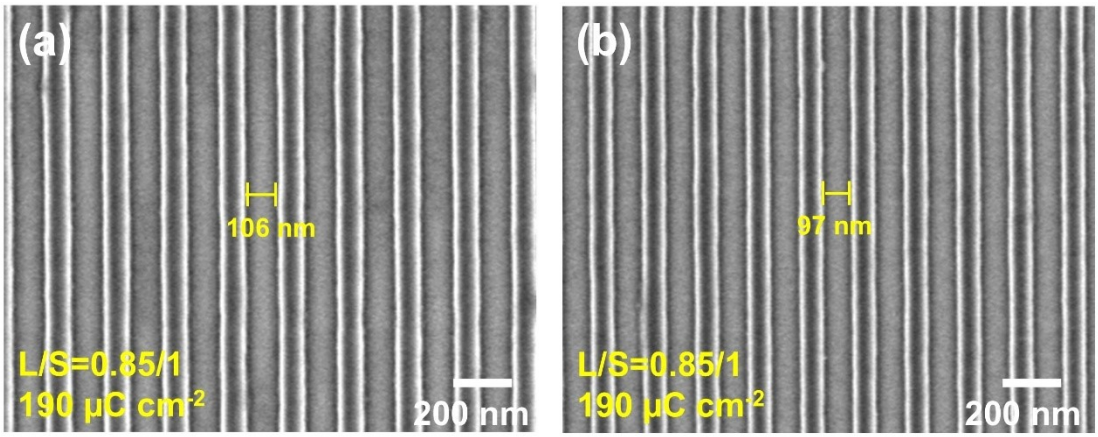

Fig. S26. SEM images of PR-1d photoresist at exposure dose of 190 μC cm^{-2}. (a) Space = 106nm (Pitch = 200 nm, L/S = 1/1); (b) Space = 97nm (Pitch = 180 nm, L/S = 1/1). (PEB at 110 ℃ for 30 s and development in TMAH for 60 s).

10. Summary of reported PAGs

Table S5. Summary of Φ_a, photoresist formulations, and lithography performance of recently reported PAGs.

ıes	Φ_a	Photoresist formulations		Lithography performance					
				365 nm	254/ 248 nm	EBL			
						Sensitivity (μC cm^{-2}) / Contrast	Isolated lines resolution (nm) / LER (nm) / Dose (μC cm^{-2})	Dense patterns resolution (nm HP) / LER (nm) / Dose (μC cm^{-2})	Volt (k
PySO	-	P(E-G) + 10%TFPSO + 10%ITX		√	-	-	-	-	-
		PMAM + 5%PAG-1		-	-	35.13 / 3.58	89.94 / - / 17	-	
G-X	-	PAG-bound	PB-1	-	-	120.73 / 13.96	71.07 / - / 131	-	
			PB-2	-	-	109.39 / 7.63	55 / 3.87 / 133	-	3
			PB-5	-	-	113.88 / 11.27	70.95 / - / 114	-	
			PB-6	-	-	74.64 / 6.31	42 / 3.6 / 73	-	
			PB-7	-	-	61.01 / 3.77	52 / 3.71 / 65	-	
nate Ester le (OMe-X)	9.073~16.339	-		-	-	-	-	-	-
ıionic ıated PAGs	38.8~41.6	PMAM + NIOPf		√	-	~15 / ~4	123 / - / 34	-	3
		PMAM + BTOPf		-	-	~18.5 / ~3.5	70 / - / 43	-	
ene-imide ~3f)	14.5~32.6	-		-	-	-	-	-	-
ıethoxy-enzyl p - sulfonate ONS)	-	P(MONMA-HEMA-TBMA) + MONS		√	-	-	-	-	-
ate ester 3a-3f)	6.4~21.4	-		-	-	-	-	-	-
-Nf	-	MIOST + 5 wt% NI-Nf		√	-	-	-	-	-
G 1-9	-	PPA + 20 wt% PAG		-	√	-	-	-	-

Table S5. Summary of Φ_a, photoresist formulations, and lithography performance of recently reported PAGs.

s	Φ_a	Photoresist formulations	Lithography performance					
					EBL			
			365 nm	254/ 248 nm	Sensitivity (μC cm^{-2}) / Contrast	Isolated lines resolution (nm) / LER (nm) / Dose (μC cm^{-2})	Dense patterns resolution (nm HP) / LER (nm) / Dose (μC cm^{-2})	Volta (kV
odonium ate	-	PASS-$N_{50\%}$ + 5 wt% PAG	-	√	4.3 / 5.1	14 / 1.3 / 0.00016	50 /- / -	20 /
TPS	-	PAG-bound (PTIMV)	-	√	-	-	-	-
-based m salts	0.88~13	-	-	-	-	-	-	-
-SS	-	PAG-bound (PTBM)	-	√	-	-	-	-
m salts	5~25	-	-	-	-	-	-	-
limide - onionic e PAG	6.2~17.6	PG + 5%PAG 1d	√	√	54.4 / 24.39	28 / 1.30 / 190	67 / 2.49 / 190	50

11. AFM characterization

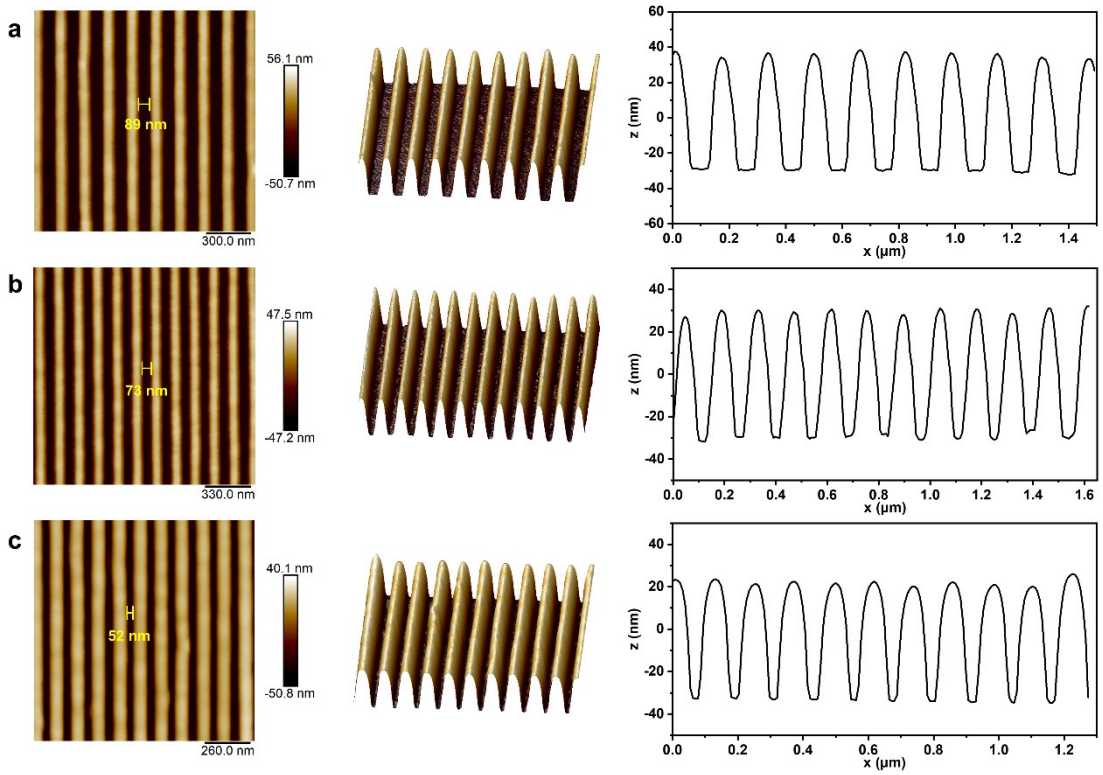

Fig. S27. Various characterization modes of AFM were used to pattern different sizes (a: 89nm, b: 73nm, and c: 52nm) of PR-1d photoresist. (from left to right: 2D morphology, 3D view, line profile height curve)

References

1. L. T. Zhou, Z. X. Tang, H. Y. Li, H. S. Xin and J. H. Zhang, Enhancing 365 nm Photoresist Performance Using 2-Isopropylthioxanthone as a Photosensitizer, *ACS Appl. Mater. Interfaces*, 2025, **17**, 39542-39551.
2. Y. Liu, D. Wang, H. Wang, H. Chen, Q. Wang and W. Kang, Enhanced Lithography Performance with Imino/Imido Benzenesulfonate Photoacid Generator-Bound Polymer Resists, *Small*, 2025, **21**, 2412297.
3. W. Zhang, M. Yang, H. Zhu, J. Li, L. Yuan, L. Yao, Y. Su and W. Li, Electronic Effects and Steric Effects for the Design of N-Sulfonate Ester Phthalimide Photoacid Generators with High Acid Production Efficiency and Thermal Stability, *Phys. Chem. C*, 2024, **128**, 19883-19892.
4. Y. Liu, D. Wang, Q. Wang and W. Kang, Polymerizable Nonionic Perfluorinated Photoacid Generators for High-Resolution Lithography, *Small Methods*, 2024, **8**, 2400112.
5. L. Zhang, B. Feng, S. Pang, H. Xin, K. Li and Y. Jin, Synthesis and performance study of nonionic photoacid generators based on Norbornene-imide, *J. Mol. Struct.*, 2024, **1304**, 137653.
6. L.-Y. Peng, S.-L. Xiang, J.-D. Huang, Y.-Y. Ren, P. Hong, C. Li, J. Liu and M.-Q. Zhu, Dual nonionic photoacids synergistically enhanced photosensitivity for chemical amplified resists, *Chem. Eng. J.*, 2024, **482**, 148810.
7. Q. Sun, B. Feng, Z. Sun, R. Liu, H. Ding and Y. Jin, Synthesis and properties of a series of sulfonate ester photoacid generators, *React. Chem. Eng.*, 2024, **9**, 630-641.
8. Y. Ku, K. Kim, H.-T. Oh, B.-G. Park, S. Lee, J.-K. Lee, C. Koh, T. Nishi and H.-W. Kim, Extreme UV Resist Exhibiting Synergism between Chemical and Physical Crosslinking Mechanisms, *Langmuir*, 2023, **39**, 3462-3470.
9. J. Deng, S. Bailey, S. Jiang and C. K. Ober, High-Performance Chain Scissionable Resists for Extreme Ultraviolet Lithography: Discovery of the Photoacid Generator Structure and Mechanism, *Chem. Mater.*, 2022, **34**, 6170-6181.
10. R.-S. Zhang, L. Miao, X.-Y. Lu, Q. Li, F. Luo, H.-Y. Qiu and G.-P. Wu, Norbornene and Epoxide-Substituted Silsesquioxane Photoresists with High-Sensitivity and Stability, *ACS Nano*, 2025.
11. N. Qin, N. Li and X. Gao, Enhanced lithographic performance of polymer-bound PAG photoresists synthesized via RAFT polymerization, *Polym. Chem.*, 2025, **16**, 841.
12. F. Petko, M. Jankowska, M. Galek, M. Noworyta, R. Popielarz and J. Ortyl, One-Component Stilbene-Based Iodonium Photoinitiators with Increased Photoacid Quantum Yield for Cationic Vat 3D Printing, *Macromolecules*, 2024, **57**, 11639-11657.
13. H. M. Yu, S. S. Liu, H. Y. Fu, Z. P. Cui, L. S. Zhang and J. Tian, POSS and PAG Dual-Containing Chemically Amplified Photoresists by RAFT Polymerization for Enhanced Thermal Performance and Acid Diffusion Inhibition, *Appl. Sci.-Basel*, 2024, **14**, 7722.
14. Y. Wang, G. Sheng, J. Xie, D. Wan and M. Jin, Push–pull biphenyl–based iodonium salts: Highly sensitive one-component photoinitiators for photopolymerization under UV–visible LEDs, *Prog. Org. Coat.*, 2024, **188**, 108209.